REFOLDING AND CHARACTERIZATION OF METHIONINE ADENOSYLTRANSFERASE FROM *Euglena gracilis*

Francisco Garrido[1], Sylvie Estrela[1], Claudia Alves[1], Gabino F. Sánchez-Pérez[2], Antonio Sillero[1,3], María A. Pajares[1,*]

[1]Instituto de Investigaciones Biomédicas "Alberto Sols" (CSIC-UAM), Arturo Duperier 4, 28029 Madrid (Spain).

[2]Department of Biochemistry and Molecular Biology, Dalhousie University, Halifax, Canada B3H 1X5.

[3]Departamento de Bioquímica, Facultad de Medicina, Universidad Autónoma de Madrid (UAM), Arzobispo Morcillo 2, 28029 Madrid (Spain).

[*]To whom correspondence should be addressed at: Instituto de Investigaciones Biomédicas "Alberto Sols" (CSIC-UAM), Arturo Duperier 4, 28029 Madrid, Spain. (Phone: 34-915854414; FAX: 34-915854401; email: mapajares@iib.uam.es)

Keywords

Methionine adenosyltransferase, inclusion bodies, refolding, characterization, secondary structure, structural model.

Abbreviations

MAT, methionine adenosyltransferase; cMAT, methionine adenosyltransferase from *E. coli*; BsMAT, methionine adenosyltransferase from *B. subtilis*; MAT I, mammalian methionine adenosyltransferase tetramer; MAT III, mammalian methionine adenosyltransferase dimer; MAT II, mammalian methionine adenosyltransferase heterotetramer; Mj-MAT, methionine adenosyltransferase from *Methanococcus jannaschii*; MATα1, MAT I/III catalytic subunit; AdoMet, S-adenosylmethionine.

ABSTRACT

Methionine adenosyltransferase from *Euglena gracilis* (MATX) is a recently discovered member of the MAT family of proteins that synthesize S-adenosylmethionine. Heterologous overexpression of MATX in *Escherichia coli* rendered the protein mostly in inclusion bodies under all conditions tested. Therefore, a refolding and purification procedure from these aggregates was developed to characterize the enzyme. Maximal recovery was obtained using inclusion bodies devoid of extraneous proteins by washing under mild urea (2 M) and detergent (5%) concentrations. Refolding was achieved in two steps following solubilization in the presence of Mg^{2+}; chaotrope dilution to <1 M and dialysis under reducing conditions. Purified MATX is a homodimer that exhibits Michaelis kinetics with a V_{max} of 1.46 μmol/min/mg and K_m values of approximately 85 and 260 μM for methionine and ATP, respectively. The activity is dependent on Mg^{2+} and K^+ ions, but is not stimulated by dimethylsulfoxide. MATX exhibits tripolyphosphatase activity that is stimulated in the presence of S-adenosylmethionine. Far-UV circular dichroism revealed β-sheet and random coil as the main secondary structure elements of the protein. The high level of sequence conservation allowed construction of a structural model that preserved the main features of the MAT family, the major changes involving the N-terminal domain.

INTRODUCTION

Reactions using S-adenosylmethionine (AdoMet) are among the most abundant processes taking place in any cell [1,2]. The routes in which the AdoMet-consuming reactions are involved allow the synthesis of a large variety of compounds, as well as the control of cell function (i.e. epigenetic modifications). This wide use of AdoMet derives from the variety of groups that this molecule is able to donate, being methyl group donation the main consumer of the compound [2-5]. In contrast, methionine adenosyltransferases (MATs) are the only enzymes known to synthesize AdoMet in a rather unusual reaction that occurs in two steps [6,7]. First, the substrates methionine and ATP are combined to obtain AdoMet and triphosphate that is hydrolyzed in the second part of the reaction to render pyrophosphate and inorganic phosphate as side products. The catalytic mechanism followed is of the S_N2 type and most of the inorganic phosphate obtained derives from the γ-phosphate of ATP [6,7]. MATs require divalent cations (Mg^{2+}) for catalysis and are activated by monovalent ions (K^+). In mammals, AdoMet has a dual behavior on MATs, inhibiting (MAT I and II) and activating (MAT III) its own synthesis, and enhancing the tripolyphosphatase activity [2,8,9].

MAT enzymes have been found in almost every organism from *Mycoplasma genitalium* to mammals with the exception of a few parasites that obtain AdoMet from their hosts [10]. For this purpose, AdoMet transporters are required and proteins exhibiting such function have been identified in some organisms, as well as in yeast and mammalian mitochondria [11-13]. Most organisms express several MAT isoenzymes that differ in their affinities for the substrates (30 μM to 1 mM for methionine in mammals), despite the high conservation of the sequences of their catalytic subunits [2,7,14]. Most members of the MAT family are homo-oligomers except for mammalian MAT II, and the majority are tetramers with the exception of a few dimers (i.e. mammalian MAT III and archaeal

MATs) [7,15]. All the crystal structures known to date (mammalian and *E. coli* MATs) show monomers organized in three domains formed by nonconsecutive stretches of the sequence, and the subunits interact through a large flat hydrophobic surface to form the dimers [7,16-18]. Active sites, two per dimer, locate between monomers with residues of both subunits contributing to them, thus the minimum association level of active MATs is the dimer. Sequence and structural restrictions to maintain the relative positions of the active site residues, and the unusual reaction mechanism, impose that the insertions and deletions observed in specific lineages take place mostly in the loops [10]. Moreover, these indels are conserved in the lineages in which they occur as observed in the analysis carried out in Bacteria and Eukarya. Recently, a different type of eukaryotic MAT (MATX) was identified in dinoflagellates, haptophytes, diatoms and euglenids [19,20]. This new MAT preserves the catalytic residues, its sequence contains insertions/deletions in loops and it is able to complement the corresponding *Saccharomyces cerevisiae* mutant, thus demonstrating its capacity to synthesize AdoMet [21]. Several species express both a canonical MAT and this new MATX, hence raising the possibility that the characteristics of each isoenzyme favor adaptation to the growth conditions or the diverse needs during the life cycle of the organism. The purpose of this article is to fully characterize MATX and compare its properties with those of other members of the MAT family. Differences in the active sites among MATs may provide the basis for the use/design of inhibitors for selective growth control of certain organisms, and hence the infections they produce that may have important pathological or commercial consequences.

MATERIALS AND METHODS

Materials

Methinonine, ATP, S-adenosylmethionine (AdoMet) dithiothreitol (DTT), ampicillin, molecular mass standards for gel filtration chromatography and protease inhibitors were obtained from Sigma Chemical Company (St. Louis, MO). [2,8-^{3}H]-ATP (28.7 Ci/mmol), Pfu DNA polymerase and restriction enzymes were products of Perkin Elmer (Boston, MA), Biotools (Madrid, Spain) and Invitrogen (Carlsbad, CA), respectively. Q-Sepharose HiTrap and Superose 12 10/300 GL columns were purchased from GE Healthcare (Uppsala, Sweden). Isopropyl β-D-thiogalactopyranoside (IPTG) and *E. coli* strains were products of Calbiochem (La Jolla, CA) and Stratagene (La Jolla, CA), respectively. Electrophoresis reagents and the BioRad protein assay kit were obtained from BioRad (Richmond, CA). YM-30 ultrafiltration membranes were purchased from Amicon Corp. (Beverly, MA). Urea, DMSO and Triton X-100 were products from Merck (Darmstadt, Germany). The rest of the buffers and reagent were from the best quality commercially available.

Construction of MATX expression plasmids

The ORF of MATX was amplified by PCR from the pEXT5-MATX plasmid provided by Dr. A. Rogers's laboratory. For this purpose, primers that include NdeI (5'-GGAATTCCATATGGCTGAATCTGCTTCAAAG-3') and EcoRI (5'-GCGAATTCCTA GTCCACCCACTTCTG-3') restriction sites (underlined) were designed. Following an initial denaturation step at 95ºC for 2 min, amplification was performed for 30 cycles at 95ºC for 30 s, 55ºC for 1 min and 72 ºC for 1 min using Pfu DNA polymerase. The PCR also included a final elongation step at 72ºC for 10 min. The PCR fragment was then

purified, digested and cloned into the pT7.7 vector [22] using the NdeI and EcoRI restriction sites. The resulting plasmid was designated pT7.7-MATX. The sequence was verified by automatic sequencing at the facilities of the Instituto de Investigaciones Biomédicas "Alberto Sols".

MATX overexpression in E. coli

The pT7.7-MATX plasmid was transformed into BL21(DE3) Codon Plus competent cells and single colonies were grown in LB medium (500 ml) containing 50 μg/ml ampicillin at 20ºC, 30ºC and 37ºC. The cell density was measured and aliquots (25 ml) taken and induced at A_{600}=0-0.8 using 0.5 mM IPTG for 0-22 h. Cells were harvested by centrifugation and stored at -80ºC until processing.

Analysis of soluble and insoluble fractions

Cell pellets (1 g wet wt) were lysed by sonication at 4ºC in a Soniprep 150 sonifier (15 cycles, 30 s on/off at an output power level of 8 microns) in 25 ml of 50 mM Tris/HCl pH 8, 10 mM $MgSO_4$ (buffer A) containing 5 mM EDTA, 0.1 % 2-mercaptoethanol, 2 μg/ml aprotinin, 1 μg/ml pepstatin A, 0.5 μg/ml leupeptin, 2.5 μg/ml antipain, 0.5 mM benzamidine, 0.1 mM phenylmethylsulfonyl fluoride (PMSF). Soluble and insoluble fractions were separated by centrifugation at 13000g for 15 min. The insoluble fraction, containing the inclusion bodies, was solubilized in 10 ml of 50 mM Tris/HCl pH 8, 75 mM $MgSO_4$ containing 8 M urea and aliquots prepared for SDS-PAGE. In parallel, soluble fractions were used for both SDS-PAGE and activity measurements.

MATX refolding from inclusion bodies

The insoluble fraction obtained from 1 g of cells was resuspended in 25 ml of buffer A containing 1 mM EDTA and sonicated again 6 cycles (10 s on/off, output power 8 microns) on ice. Pellets were recovered by centrifugation for 30 min at 48000g and 4ºC. These pellets were used to test washing conditions using 100 mM Tris/HCl pH 7 buffers including 5 mM EDTA, 0-4 M urea, 0-5 % Triton X-100 and 0.1 mM benzamidine. These washes were carried out twice, followed by a final wash with the same buffer devoid of urea and detergent.

One washed pellet was resuspended in 10 ml of 50 mM Tris/HCl pH 8 containing 8 M urea and 75 mM $MgSO_4$ and incubated for 2 hours at 10ºC. Thereafter the sample was diluted to reach 0.5-4 M urea by addition of buffer A. Each diluted sample was immediately dialyzed against buffer A containing 10 mM DTT (total volume 1.5 l). Refolded MATX was recovered by centrifugation of the dialyzed samples for 30 min at 48000g and 4ºC, and checked for MAT activity and protein.

Purification of refolded MATX

Refolded MATX was purified using Q-Sepharose HiTrap (5 ml) equilibrated in buffer A containing 0.1 % 2-mercaptoethanol and 0.1 mM benzamidine. The flow rate was 1 ml/min and 5 ml fractions were collected. Following sample loading an extensive washing step (100 ml) was carried out using buffer A until A_{280}=0. Elution was performed with a gradient from 0-0.5 M KCl in buffer A (150 ml) at the same flow rate. The presence of MATX was detected by activity measurements and the corresponding peak collected and dialyzed against buffer A to eliminate KCl excess or against 50 mM Tris/HCl pH 8 for Mg^{2+} kinetics. In some cases, the peak was concentrated by ultrafiltration using YM-30 membranes until the desired protein concentration was reached.

Far and near UV circular dichroism

MATX samples were prepared at 0.25 mg/ml and 1 mg/ml protein concentrations for far- and near-UV CD, respectively. Spectra were recorded on a Jasco J-720 spectropolarimeter at 25ºC, using 0.1 cm (far-UV) or 1 cm (near-UV) pathlength cuvettes. After baseline subtraction the observed ellipticities were converted to mean residue ellipticities (θ_{mrw}) on the basis of a mean molecular mass per residue of 110 Da. A minimum of five spectra was taken for each sample. Analysis of secondary structure was performed using the deconvolution software CDNN (© G. Böhm).

Sedimentation velocity

MATX samples (0.3-0.5 mg/ml) were used for sedimentation velocity runs that were carried out at 48000 rpm and 4ºC in an XL-1 analytical ultracentrifuge (Beckman Coulter, Inc., Fullerton, CA) with a UV-Vis detection system, using an An50Ti rotor and 12 mm double-sector centerpieces. Absorbance scans (0.003 cm step size) were taken at 280 nm. Differential sedimentation-coefficient distributions, *c(s)*, were calculated by least squares boundary modeling of sedimentation velocity data using the program SEDFIT [23,24]. The values obtained from this analysis were corrected for solvent composition and temperature to obtain $s_{20,w}$ using the public domain software SEDNTERP, retrieved from the RASMB server [25].

Analytical gel filtration chromatography

MATX samples (100 µl containing a minimum of 50 µg) were injected on a Superose 12 10/300 GL gel filtration column equilibrated in buffer A containing 150 mM KCl. The flow rate was 0.3 ml/min and 210 µl fractions were collected while A_{280} was recorded. Elution and MAT activity measurements (100 µl) were performed as previously

described [26]. The protein standards used and their elution volumes were as follows: Dextran Blue (2000 kDa), 8.69 ml; apoferritin (443 kDa), 9.87 ml; β-amylase (200 kDa), 11.34 ml; alcohol dehydrogenase (150 kDa), 12.07 ml; carbonic anhydrase (29 kDa), 15.12 ml; and ATP (0.551 kDa), 19.26 ml.

Electrophoresis

Denaturing gel electrophoresis was performed on 10% SDS-PAGE gels under reduced conditions, using the Laemmli buffer system. Samples of soluble (150 μg), inclusion bodies (30 μg) and refolded MATX (6 μg) were loaded per lane and stained using Coomassie blue R250. Densitometric scanning of the bands was carried out using the ImageJ software 1.37v (http://rsb.info.nih.gov/ij/).

MAT activity measurements and kinetics

Activity assays were carried out at 37ºC as previously described [27], using a protein concentration of 0.05 mg/ml and the standard MAT reaction mixture containing 5 mM methionine and 5 mM ATP in a final volume of 250 μl. Kinetics were performed using standard MAT reaction mixtures containing: i) 1-600 μM of the amino acid and 5 mM ATP, for methionine kinetics; ii) 1-1500 μM of the nucleotide and 5 mM methionine, for ATP kinetics; iii) 0-13 mM $MgSO_4$, for Mg^{2+} kinetics; and iv) 0-85 mM KCl, for K^+ kinetics. DMSO stimulation was tested using reaction mixtures containing 60 μM methionine and 10% (v/v) DMSO.

Tripolyphosphatase activity measurements

MATX tripolyphosphatase activity was measured following absorption at 750 nm as previously described [17]. Tripolyphosphate kinetics were carried out using 0-5 mM

triphosphate in the presence or absence of 50 μM AdoMet and using 0.05 mg/ml protein samples.

Theoretical calculations of the pI and extinction coefficient.

Information from the amino acid sequence was used for theoretical calculation of the pI using a method previously described by Ribeiro and Sillero [28]. In addition, the extinction coefficient was estimated from the number of tryptophan and tyrosine residues in the sequence, and using extinction coefficients for these amino acids of 5550 and 1490 $M^{-1}cm^{-1}$, respectively.

Protein concentration determinations

The protein concentration of the samples was measured routinely using the BioRad protein assay kit and bovine serum albumin as the standard. On the other hand, for CD and sedimentation velocity experiments protein concentration was determined from the A_{280} of the sample after 30 min incubation in 8 M urea using a calculated extinction coefficient of 48610 $M^{-1}cm^{-1}$.

MATX structural model and sequence alignment.

A structural model of the MATX monomer was prepared using the Swiss-Model server (http://swissmodel.expasy.org/), the protein sequence and the 2.05 Å resolution structure of the human MATα1 protein (PDB ID: 2OBV) as template (49.5% sequence identity)[29-31]. The model extends from residue 13 to 444 of the sequence and preserves the three-domain organization of all the previously crystallized MATs [7,16,17]. Sequence alignment of the MATs mentioned in the text was performed using the COBALT Multiple Alignment Tool (http://www.ncbi.nlm.nih.gov/tools/cobalt).

RESULTS AND DISCUSSION

MATX from *Euglena gracilis* belongs to the MAT family of enzymes characterized by the high level of sequence identity exhibited by its members [10]. Its ORF encodes for a protein of 471 residues, which means a notable increase in length as compared to most MATs (~400 amino acids long). MATX has a theoretical pI of 5.91, similar to the values obtained to date for most members of the family (i.e. 5.9 for rat MAT III) [7,32]. Heterologous expression of the protein was initially carried out in *E. coli* using the plasmid pEXT5-MATX, which includes a His-tag at the protein N-terminal. However, the expression levels obtained were very low under all the conditions tested (growth temperature, cell density for induction, etc.). Addition of tags to other MATs, both at the N- or C-terminal ends, was previously shown to decrease the amount of soluble protein obtained [33], and hence the pT7.7-MATX plasmid that contains the MATX ORF without the His-tag was constructed. Growth and induction conditions of *E. coli* cells transformed with pT7.7-MATX were studied and optimized. The protein appeared in 10% SDS-PAGE gels with a calculated Mr of 57600, according to the mobility of the standards (Fig. 1), which is slightly above the calculated size. MAT activity was higher in soluble fractions of cultures induced at A_{600}= 0.8 (Fig. 2), although no significant changes in the protein band intensity were detected by densitometric scanning of the stained gels (Fig. 1A). Overexpression of MAT enzymes produces a large decrease in cellular ATP levels, as its consumption is increased to produce AdoMet. Thus, it is possible that only low levels of expression allow cell survival, and hence that a larger cell number may led to an apparent constant level of MATX once a certain density is achieved, whereas the activity levels increase due to a larger contribution of the endogenous cMAT. The activity was also increased in soluble fractions of cultures grown at 30ºC as compared to those grown at 37ºC (Fig. 3). Maximum induction with IPTG was already detected after a 3 h induction

period at both temperatures. However, in all the conditions tested most of the protein (~90%) was accumulated in inclusion bodies (Fig. 1B). The use of lower temperatures (20ºC) and IPTG concentrations was reported to improve *Bacillus subtilis* MAT (BsMAT) heterologous expression [34]. In our hands none of these conditions improved the results obtained and in fact the soluble protein was almost undetectable (data not shown). Therefore, the standard grown conditions were established to obtain MATX from inclusion bodies using 3 h IPTG induction at A_{600}=0.6-0.8 and 37ºC and refolding from inclusion bodies was attempted.

Several parameters were studied using the inclusion bodies, in order to obtain the maximum amount of protein for refolding. These included the protein concentration, pH of the buffer and the concentrations of the solubilization agents, as previously described for mammalian MAT I/III refolding [32]. Inclusion bodies contain not only the desired overexpressed protein, but also bacterial membrane and cell wall and therefore the need to eliminate these extraneous proteins. For this purpose, the inclusion bodies were subjected to several washing steps with buffers including variable concentrations of urea (0-4 M) and Triton X-100 (0-5%) at pH 7. In contrast to MAT I/III, with a similar pI [32], a large amount of MATX was solubilized when using washing buffers containing >2 M urea, whereas the percentages of detergent examined did not cause such protein loss. Therefore, the standard washing conditions were established as two washes in the presence of 2 M urea and 5% Triton X-100.

Refolding of MATX from the washed inclusion bodies was then attempted. For this purpose, the protein was solubilized using a buffer containing 8 M urea, and the refolding protocol previously developed for rat MAT I/III [32]. However, for this protocol to be adapted to MATX several requirements had to be tested. First, the range of protein concentration at the solubilization step that renders the largest amount of active refolded

MATX. According to the results obtained, this protein concentration was established between 1-3 mg/ml. Secondly, the intermediate urea concentration to be reached in the dilution step. This dilution was found to dramatically improve the yield of active-refolded MAT I/III [32], and hence expected to be crucial for MATX refolding. Our results indicate that achieving a urea concentration between 0.5-1 M before dialysis, and hence a protein concentration of 0.1-0.3 mg/ml, allowed the largest recovery of active protein (Fig. 4). Finally, the presence of 10 cysteine residues in the MATX sequence, and the crucial role that this type of amino acids have in all MATs studied to date [7,35,36], recommends the inclusion of a reducing agent in the dialysis buffer to avoid the production of off-pathway aggregates due to oxidation. Based on the data obtained, an intermediate dilution to 1 M urea followed by dialysis in the presence of 10 mM DTT was used as the standard procedure.

The refolded protein was further purified by ion exchange chromatography, and a single peak exhibiting MAT activity eluted in the presence of 100 mM KCl. The MATX content of this preparation was estimated to be >90% by densitometric scanning of the stained gels (Fig. 5). The purification results appear in Table 1, and show a remarkably lower yield at the dialysis step as compared to MAT I/III (25 vs. 88%) [32]. Given the high sequence identity level between MATs this result was unexpected, and demonstrated how highly homologous proteins can behave quite differently under similar conditions.

This highly purified MATX preparation was then used for characterization. The oligomeric state of the refolded protein was analyzed using gel filtration chromatography and sedimentation velocity. The elution volume of MATX (13.2 ml) was determined from MAT activity measurements of the fractions eluted from the gel filtration column (Fig. 6). According to the elution position of the markers on the Superose column, this elution volume corresponds to that expected for a globular protein of ~70 kDa. However, the A_{280}

profile indicates elution of the protein as two peaks in positions compatible with tetrameric and dimeric oligomers. In addition, sedimentation velocity experiments identify species with calculated $s_{20,w}$ values of 3.4 ± 0.1 and 6.4 ± 0.1 S. These hydrodynamic measurements are compatible with the presence in the sample of monomers (compact or globular) and compact dimers, according to the A_{280} measurements of sedimentation velocity experiments, from which only compact dimers were active as deduced from the gel filtration chromatography profile. Detection of tetrameric species could be ascribed to a partial association during sample concentration preceding gel filtration chromatography, whereas that of monomeric species could be due to partial denaturation of the sample during ultracentrifugation, phenomena described to occur with a variety of enzymes [37,38]. As deduced from these data, MATX is a new member of the growing group of homodimeric MATs that includes mammalian MAT III, archaeal MATs and *Mycobacterium tuberculosis* MAT [7,15,35,39,40]. The AdoMet synthesizing activity of some of these dimeric MATs is stimulated by DMSO at low methionine concentrations [7]. Therefore, we analyzed this stimulatory effect on MATX and found that this dimeric MAT is not stimulated under similar conditions (1.80 ± 0.15 vs. 1.67 ± 0.11 μmol/min/mg).

MAT activity is dependent on divalent (Mg^{2+}) cations and stimulated by monovalent (K^{+}) ions [7], and MATX is not an exception to this rule. Its dependence on these essential cations was explored and the data obtained appear in Table 2. The affinity for the cations is in the millimolar range, similar values to those measured for refolded MAT III [32]. Kinetics for the substrates, methionine and ATP, showed Michaelis-Menten behavior, the calculated K_m values being about half of those exhibited by MAT III (Table 2)[32]. In addition, the V_{max} is ~18 fold higher than that of MAT III [32], and similar to that of *E. coli* MAT (cMAT)[6] or *Methanococcus jannaschii* MAT (Mj-MAT)[40]. The

tripolyphosphatase activity exhibited by the MAT family was also evaluated for MATX. Kinetics for PPP_i showed a V_{max} for this substrate similar to that shown by refolded-MAT III in the presence of 50 μM AdoMet [32]. MATX tripolyphosphatase activity was stimulated by AdoMet ~23 fold, rendering a calculated V_{max} ~2 fold larger than that of the AdoMet synthesis reaction as occurs for cMAT [6] (Table 2). However, this 2-fold increase in V_{max} (1464.22 vs 2725.20 nmol/min/mg) is also observed when the AdoMet synthesis is measured as P_i using the colorimetric method (3349.33 ± 71.61 nmol/min/mg). This stimulation occurs without a significant change in affinity for the PPP_i substrate (Table 2), in contrast to the decreased affinity shown by cMAT in the presence of AdoMet (~4 fold)[6].

Structural characterization of refolded MATX was carried out using circular dichroism. Far-UV spectra were obtained (Fig. 7) and the overall secondary structure composition estimated by deconvolution (Table 3). The major elements were found to be the random coil and β-sheet as previously described for other members of the MAT family. Comparison of these data with the secondary structure composition published for other members of the MAT family showed an increase in the random coil component that is especially important when compared to archaeal or BsMAT [32,34,41]. The difference in subunit length between these MATs (471 vs. 400 residues)(Fig. 8C), and the fact that the insertions occur in loops [19], may account for such increased random coil content. In addition, some differences can also be expected from the diversity of programs used in this type of calculations by each laboratory. Near-UV spectra were also obtained (Fig. 7B), the main feature being the lack of signal at 265 and 295 nm. MATX contains five tryptophans (positions 181, 182, 314, 437 and 469) and fourteen tyrosines (positions 78, 148, 162, 195, 232, 311, 336, 360, 375, 413, 419, 434, 446 and 449) per subunit, two types of residues with transitions in this area of the spectrum. Hence, a compensatory effect between signals

of both types of residues must occur to render this profile. Such a compensatory effect has been previously observed in near-UV CD spectra from Mj-MAT (containing 1 Trp and 13 Tyr), despite the low degree of sequence conservation in archaeal MATs [41]. Moreover, the absence of a significant signal in the 250-270 nm range suggested the lack of disulphide bonds in the molecule, as expected from refolding being carried out under reducing conditions.

The sequence of MATX preserves the main blocks that characterize all the members of this family and that include the residues involved in substrate and cation binding (Fig. 8C) [10]. Residues involved in methionine binding locate to the N-terminal domain, the ^{27}GHPDK^{31} stretch (block I), and to a loop connecting this domain with the central domain that includes F^{290}. This phenylalanine is equivalent to F^{251} of rMATα1 that was shown to have its aromatic ring stacked against the methionine analogue used for crystallization [17]. D^{141} (block III), D^{186} and K^{188} (block IV) are equivalent to the residues involved in Mg^{2+} binding and catalysis. Moreover, residues involved in K^{+} coordination, G^{303} and R^{305}, are also preserved (block V). Overall the sequence presents a high level of conservation, the main difference being the ~30 residue extension at the C-terminal end and an insertion comprising residues 218-248 according to the sequence alignment (Fig. 8C). This high conservation allowed construction of a structural model using the MATX sequence and the structure of human MATα1 (PDB ID: 2OBV), its closest homologue. This model extended from residue 13 to 444 and preserved the three-domain organization of all MATs (Fig. 8). The main differences occur in the N-terminal domain, where the strands of the β-sheet seem longer, as well as the loop (residues 259-281) preceeding the last strand. In addition, one of the α-helixes in the outer side of this domain is also longer (residues 234-259), thus protruding to the environment. However, these changes do not

seem to affect positioning of the active site residues as compared with rMATα1 (Fig. 8A)[17,41], and hence the high activity observed comparable to that of cMAT.

In summary, we have been able to produce and refold MATX using an heterologous system. The enzyme is a homodimer showing AdoMet synthesizing capacity, but its V_{max} and the affinities displayed for ATP and methionine are closer to those of the cMAT homotetramer rather than to Mj-MAT or rMAT III dimers. MATX activity is also dependent on divalent and monovalent cations. Moreover, the enzyme exhibits the tripolyphosphatase activity typical of the MAT family that is stimulated in the presence of AdoMet.

ACKNOWLEDGEMENTS

S. E. and C. A. were fellows of the Erasmus Program from Porto University (Portugal). This work was supported by grants of the Ministerio de Ciencia e Innovación (BFU2008-00666 and BFU2009-08977 to M.A.P.). The authors wish to thank Dr. A. Martínez del Pozo from the Dept. of Bioquímica y Biología Molecular I of the Universidad Complutense de Madrid for his help with CD spectra, Dr. A. Rogers from the Dalhousie University (Canada) for the pEXT5-MATX plasmid and Brenda Ashley Morris for style and grammatical corrections.

REFERENCES

[1] J.R. Sufrin, S. Finckbeiner, C.M. Oliver, Marine-derived metabolites of S-adenosylmethionine as templates for new anti-infectives, Mar. Drugs 7 (2009) 401-434.
[2] J.M.Mato, L. Alvarez, P. Ortiz, M.A. Pajares, S-adenosylmethionine synthesis: molecular mechanisms and clinical implications, Pharmacol. Ther. 73 (1997) 265-280.
[3] D.F. Iwig, S.J. Booker, Insight into the polar reactivity of the onium chalcogen analogues of S-adenosyl-L-methionine, Biochemistry 43 (2004) 13496-13509.

[4] M. Fontecave, M. Atta, E. Mulliez, S-adenosylmethionine: nothing goes to waste, Trends Biochem. Sci. 29 (2004) 243-249.
[5] G.L. Cantoni, Biological methylation: selected aspects, Annu. Rev. Biochem. 44 (1975) 435-451.
[6] G.D. Markham, E.W. Hafner, C.W. Tabor, H. Tabor, S-Adenosylmethionine synthetase from Escherichia coli, J. Biol. Chem. 255 (1980) 9082-9092.
[7] G.D. Markham, M.A. Pajares, Structure-function relationships in methionine adenosyltransferases, Cell. Mol. Life Sci. 66 (2009) 636-648.
[8] J. De La Rosa, J. Ostrowski, M.M. Hryniewicz, N.M. Kredich, M. Kotb, H.L. LeGros Jr., M. Valentine, A.M. Geller, Chromosomal localization and catalytic properties of the recombinant alpha subunit of human lymphocyte methionine adenosyltransferase, J. Biol. Chem. 270 (1995) 21860-21868.
[9] H.L. LeGros Jr., A.M. Geller, M. Kotb, Differential regulation of methionine adenosyltransferase in superantigen and mitogen stimulated human T lymphocytes, J. Biol. Chem. 272 (1997) 16040-16047.
[10] G.F. Sanchez-Perez, J.M. Bautista, M.A. Pajares, Methionine adenosyltransferase as a useful molecular systematics tool revealed by phylogenetic and structural analyses, J. Mol. Biol. 335 (2004) 693-706.
[11] R.S. Stephens, et al., Genome sequence of an obligate intracellular pathogen of humans: Chlamydia trachomatis, Science 282 (1998) 754-759.
[12] C.M. Marobbio, G. Agrimi, F.M. Lasorsa, F. Palmieri, Identification and functional reconstitution of yeast mitochondrial carrier for S-adenosylmethionine, EMBO J. 22 (2003) 5975-5982.
[13] S. Merali, A.B. Clarkson Jr., S-adenosylmethionine and Pneumocystis, FEMS Microbiol. Lett. 237 (2004) 179-186.
[14] M. Kotb, N.M. Kredich, S-Adenosylmethionine synthetase from human lymphocytes. Purification and characterization, J. Biol. Chem. 260 (1985) 3923-3930.
[15] B.J. Berger, M.H. Knodel, Characterisation of methionine adenosyltransferase from Mycobacterium smegmatis and M. tuberculosis, BMC Microbiol. 3 (2003) 12.
[16] F. Takusagawa, S. Kamitori, S. Misaki, G.D. Markham, Crystal structure of S-adenosylmethionine synthetase, J. Biol. Chem. 271 (1996) 136-147.
[17] B. Gonzalez, M.A. Pajares, J.A. Hermoso, L. Alvarez, F. Garrido, J.R. Sufrin, J. Sanz-Aparicio, The crystal structure of tetrameric methionine adenosyltransferase from rat liver reveals the methionine-binding site, J. Mol. Biol. 300 (2000) 363-375.
[18] B. Gonzalez, M.A. Pajares, J.A. Hermoso, D. Guillerm, G. Guillerm, J. Sanz-Aparicio, Crystal structures of methionine adenosyltransferase complexed with substrates and products reveal the methionine-ATP recognition and give insights into the catalytic mechanism, J. Mol. Biol. 331 (2003) 407-416.
[19] G.F. Sanchez-Perez, V. Hampl, A.G. Simpson, A.J. Roger, A new divergent type of eukaryotic methionine adenosyltransferase is present in multiple distantly related secondary algal lineages, J. Eukaryot. Microbiol. 55 (2008) 374-381.
[20] R. Kamikawa, G.F. Sanchez-Perez, Y. Sako, A.J. Roger, Y. Inagaki, Expanded phylogenies of canonical and non-canonical types of methionine adenosyltransferase reveal a complex history of these gene families in eukaryotes, Mol. Phylogenet. Evol. 53 (2009) 565-570.
[21] P. Ho, K.F. Kong, Y.H. Chan, J.S. Tsang, J.T. Wong, An unusual S-adenosylmethionine synthetase gene from dinoflagellate is methylated, BMC Mol. Biol. 8 (2007) 87.

[22] S. Tabor, C.C. Richardson, A bacteriophage T7 RNA polymerase/promoter system for controlled exclusive expression of specific genes, Proc. Natl. Acad. Sci. USA 82 (1985) 1074-1078.
[23] P. Schuck, Size-distribution analysis of macromolecules by sedimentation velocity ultracentrifugation and Lamm equation modeling, Biophys. J. 78 (2000) 1606-1619.
[24] P. Schuck, M.A. Perugini, N.R. Gonzales, G.J. Howlett, D. Schubert, Size-distribution analysis of proteins by analytical ultracentrifugation: strategies and application to model systems, Biophys. J. 82 (2002) 1096-1111.
[25] T.M. Laue, B.D. Shah, T.M. Ridgeway, S.L. Pelletier, Computer-aided interpretation of analytical sedimentation data for proteins, in: S.E. Harding, A.J Rowe, J.C. Horton (Eds.), Analytical Ultracentrifugation in Biochemistry and Polymer Science, Royal Society of Chemistry, Cambridge, UK, 1992, pp. 90-125.
[26] G.F. Sanchez-Perez, M. Gasset, J.J. Calvete, M.A. Pajares, Role of an intrasubunit disulfide in the association state of the cytosolic homo-oligomer methionine adenosyltransferase, J. Biol. Chem. 278 (2003) 7285-7293.
[27] B. Gil, M.A. Pajares, J.M. Mato, L. Alvarez, Glucocorticoid regulation of hepatic S-adenosylmethionine synthetase gene expression, Endocrinology 138 (1997) 1251-1258.
[28] J.M. Ribeiro, A. Sillero, A program to calculate the isoelectric point of macromolecules, Comput. Biol. Med. 21 (1991) 131-141.
[29] K. Arnold, L. Bordoli, J. Kopp, T. Schwede, The SWISS-MODEL workspace: a web-based environment for protein structure homology modelling, Bioinformatics 22 (2006) 195-201.
[30] T. Schwede, J. Kopp, N. Guex, M.C. Peitsch, SWISS-MODEL: An automated protein homology-modeling server, Nucleic Acids Res. 31 (2003) 3381-3385.
[31] N. Guex, M.C. Peitsch, SWISS-MODEL and the Swiss-PdbViewer: an environment for comparative protein modeling, Electrophoresis 18 (1997) 2714-2723.
[32] M.C. Lopez-Vara, M. Gasset, M.A. Pajares, Refolding and characterization of rat liver methionine adenosyltransferase from Escherichia coli inclusion bodies, Protein Expr. Purif. 19 (2000) 219-226.
[33] E. Reytor, J. Perez-Miguelsanz, L. Alvarez, D. Perez-Sala, M.A. Pajares, Conformational signals in the C-terminal domain of methionine adenosyltransferase I/III determine its nucleocytoplasmic distribution FASEB J. 23 (2009) 3347-3360.
[34] V. Kamarthapu, K.V. Rao, P.N. Srinivas, G.B. Reddy, V.D. Reddy, Structural and kinetic properties of Bacillus subtilis S-adenosylmethionine synthetase expressed in Escherichia coli, Biochim. Biophys. Acta 1784 (2008) 1949-1958.
[35] M.A. Pajares, C. Duran, F. Corrales, M.M. Pliego, J.M. Mato, Modulation of rat liver S-adenosylmethionine synthetase activity by glutathione, J. Biol. Chem. 267 (1992) 17598-17605.
[36] G.D. Markham, C. Satishchandran, Identification of the reactive sulfhydryl groups of S-adenosylmethionine synthetase, J. Biol. Chem. 263 (1988) 8666-8670.
[37] R. Jaenicke, C. Noth, Structure-function relationship of mitochondrial malate dehydrogenase at high dilution and in multicomponent systems, Biol. Chem. Hoppe Seyler 368 (1987) 871-878.
[38] R. Jaenicke, I. Muiznieks, C. Aslanidis, R. Schmitt, Ultracentrifugal analysis of the quaternary structure of the raf repressor from Escherichia coli, FEBS Lett. 260 (1990) 233-235.
[39] C. Cabrero, J. Puerta, S. Alemany, Purification and comparison of two forms of S-adenosyl-L-methionine synthetase from rat liver, Eur. J. Biochem. 170 (1987) 299-304.
[40] Z.J. Lu, G.D. Markham, Enzymatic properties of S-adenosylmethionine synthetase from the archaeon Methanococcus jannaschii, J. Biol. Chem. 277 (2002) 16624-16631.

[41] F. Garrido, C. Alfonso, J.C. Taylor, G.D. Markham, M.A. Pajares, Subunit association as the stabilizing determinant for archaeal methionine adenosyltransferases, Biochim. Biophys. Acta. 1794 (2009) 1082-1090.

FIGURE LEGENDS

Fig. 1. *SDS-PAGE electrophoresis of soluble and insoluble fractions of MATX overexpressing cells.* Cultures of *E. coli* cells transformed with pT7.7-MATX were grown at 37ºC to reach several cell densities (A_{600}). At this point cultures were divided into two samples and grown for 3 additional hours in the absence (lanes 1, 2, 4 and 6) or presence (lanes 3, 5 and 7) of IPTG. The cells were harvested by centrifugation and lysed to obtain soluble and insoluble fractions. (A) Samples of the soluble (30 μl containing ~150 μg) and (B) insoluble (20 μl containing ~30 μg) fractions were loaded in SDS-PAGE gels. Induction was done at A_{600}=0 (lane 1), 0.3, (lanes 2 and 3), 0.6 (lanes 4 and 5) and 0.8 (lanes 6 and 7). The figure shows results of a typical experiment.

Fig. 2. *MAT activity in soluble fractions of cultures induced at different cell densities at 37ºC.* Cultures of *E. coli* cells transformed with pT7.7-MATX were grown at 37ºC to reach several cell densities (A_{600}). At this point cultures were divided into two samples and grown for 3 additional hours in the absence (●) or presence (■) of IPTG. The cells were harvested by centrifugation and lysed to obtain soluble and insoluble fractions. MAT activity was measured in the soluble fractions. The figure shows the mean ± SEM of a typical experiment carried out in triplicate.

Fig. 3. *MAT activity in soluble fractions of cultures induced at 30ºC or 37ºC.* Cultures of *E. coli* cells transformed with pT7.7-MATX were grown at 37ºC to reach A_{600}= 0.8. At this point cultures were divided into two samples and grown for 3 additional hours in the absence (●) or presence (■) of IPTG at 30ºC (A) or 37ºC (B). The cells were harvested by centrifugation and lysed to obtain soluble and insoluble fractions. MAT

activity was measured in the soluble fractions. The figure shows the mean ± SEM of a typical experiment carried out in triplicate.

Fig. 4. *Two step refolding of MATX from inclusion bodies.* Washed inclusion bodies were solubilized in 8 M urea buffer and incubated for 2 h at 10ºC. The samples were then diluted to achieve final urea concentrations between 0.5-4M and immediately subjected to dialysis in the presence of 10 mM DTT. Samples were recovered and clarified by centrifugation and the soluble fraction assayed for MAT activity. The figure shows the mean ± SD of a typical experiment carried out in triplicate.

Fig. 5. *SDS-PAGE of the MATX purification steps.* The figure shows a scheme of the purification steps, where the number indicates the corresponding lane of the SDS-PAGE gel. Samples (40 µl) of representative purification steps were prepared for SDS-PAGE electrophoresis under reducing conditions and loaded on a 10% acrylamide gel. The samples correspond to: washed inclusion bodies solubilized in 8 M urea buffer (lane 1); refolded MATX (lane 2); the peak eluted from the Q-Sepharose cartridge (lane 3). MATX appear as the main band stained in all the fractions with an apparent Mr of 57600 according to the standards: phosphorylase B (97400), bovine serum albumin (66200), ovalbumin (45000), carbonic anhydrase (31000) and soybean trypsin inhibitor (21500).

Fig. 6. *Gel filtration chromatography of refolded MATX.* MATX was refolded from inclusion bodies following the two-step protocol described under Materials and Methods, purified by ion exchange chromatography and dialyzed. A sample (100 µl containing ~80 µg) was injected on a Superose 12 10/300 GL column equilibrated in 50 mM Tris/HCl pH 8, 10 mM $MgSO_4$, 150 mM KCl. Elution was carried out at a flow rate of 0.3 ml/min, the A_{280} was recorded and 210 µl fractions were collected for MAT activity measurements. The elution volume of the markers was: Dextran Blue (8.69 ml); apoferritin (9.87 ml); β-

amylase (11.34 ml); alcohol dehydrogenase (12.07 ml); carbonic anhydrase (15.12 ml); and ATP (19.26 ml). The figure shows results from a typical experiment.

Fig. 7. *Far- and near-UV circular dichroism spectra of refolded MATX.* Samples of purified refolded MATX were used to obtain (A) far- and (B) near-UV circular dichroism spectra. The protein concentration of the samples was 0.25 mg/ml and 1 mg/ml for far- and near-UV spectra, respectively. After baseline subtraction the observed ellipticities were converted to mean residue ellipticities using a mean molecular mass per residue of 110 Da.

Fig. 8. *Comparison of monomer structures for rat MATα1 (crystal) and MATX (structural model) and alignment of MAT sequences.* (A) The structural model constructed using the Swiss-Model server and human MATα1 (PDB ID: 2OBV) as template is shown. The arrows indicate extensions in the N-terminal domain that affect a loop and α-helix. The active site residues appear as sticks (greencyan) over which the sequences are indicated. (B) The structure of the rat MATα1 monomer (PDB ID: 1QM4) is depicted for comparison. The position of the N-terminal residue for each monomer is also indicated. (C) Alignment of the MAT sequence mentioned in the text, including that of human MATα1 the higher homologue used for construction of the structural model.

TABLE 1

Refolding and purification of MATX[a,f]

	Total protein (mg)[d]	Total enzyme units[e]	Specific activity (nmol/min/mg)	Yield (%)
Urea solubilization[b]	91.89	0	<0.0001	100
Dialysis + DTT[c]	22.99	24.88 ± 3.98	1153.71 ± 208.02	25.02
Q-Sepharose	9.08	1.12 ± 0.39	1553.04 ± 238.61	9.88

[a]Washed inclusion bodies were used for refolding.
[b]Solubilization in the presence of 8 M urea for 2 h at 10ºC .
[c]The diluted sample was dialyzed against buffer A containing 10 mM DTT.
[d]Protein concentration was determined by Bradford protein assay.
[e]One unit is the amount of enzyme that catalyzed the production of 1 μmol AdoMet per minute.
[f]The table shows results of a typical purification.

TABLE 2

Kinetic parameters of MATX activities

		MATX
MAT activity[a]	V_{max} (nmol/min/mg)	1464.22 ± 164.26
	K_m methionine (μM)	85.35 ± 28.42
	K_m ATP (μM)	260.36 ± 38.90
	K_m K^+ (μM)	591.31 ± 76.64
	K_m Mg^{2+} (mM)	1.72 ± 0.27
Tripolyphosphatase activity[b]	V_{max} (nmol/min/mg)	117.28 ± 15.73
	K_m PPP_i (μM)	82.75 ± 22.24
	V_{max} (nmol/min/mg) + 50 μM AdoMet	2725.20 ± 115.15
	K_m PPP_i (μM) + 50 μM AdoMet	130.65 ± 25.95

[a]MAT activity measurements were carried out using 0.05 mg/ml protein samples for 30 min.

[b]Tripolyphosphatase activity determinations were performed using 0.05 mg/ml protein concentrations for 10 min.

TABLE 3

Secondary structure composition of MATX[a] and comparison with other MATs

		Secondary structure (%)			
		MATX	**MAT I[b]**	**MAT III[b]**	**BsMAT[c]**
α-helix		12.7 ± 0.5	23 ± 1.8	19 ± 1.1	81
β-sheet	**antiparallel**	25.1 ± 0.5	40 ± 1.2	34 ± 2.3	8
	parallel	5.3 ± 0.5			
β-turns		21.5 ± 0.5	18 ± 1.0	20 ± 0.8	
Random coil		35.9 ± 0.5	19 ± 1.8	27 ± 0.5	11

[a]Secondary structure composition was calculated from the far-UV CD spectra using CDNN software (© G. Böhm)

[b] Calculated using the Convex Constraint method, data from reference 32

[c] Calculated using the CDpro software, data from reference 34

Figure 1

A

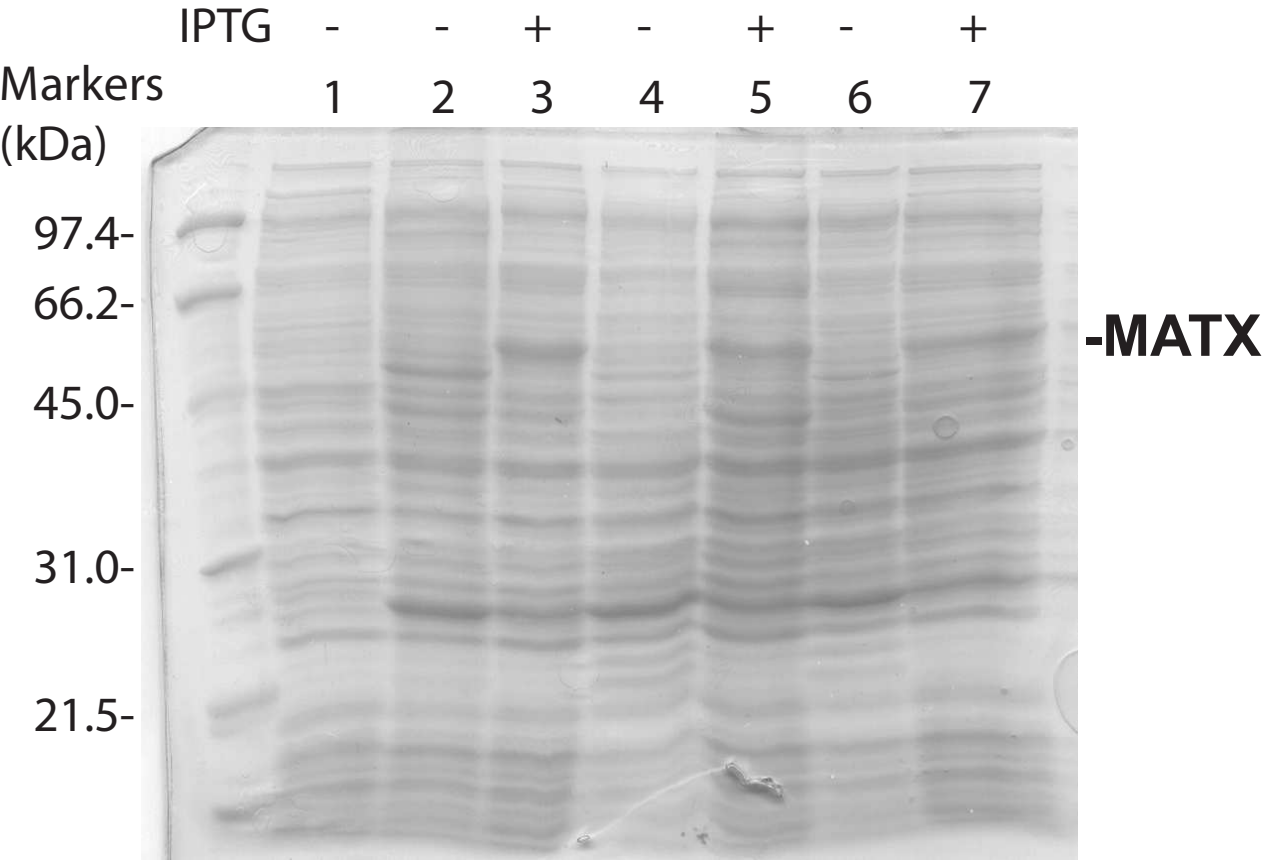
IPTG - - + - + - +
Markers
1 2 3 4 5 6 7
(kDa)
97.4-
66.2-
45.0-
31.0-
21.5-
-MATX

B

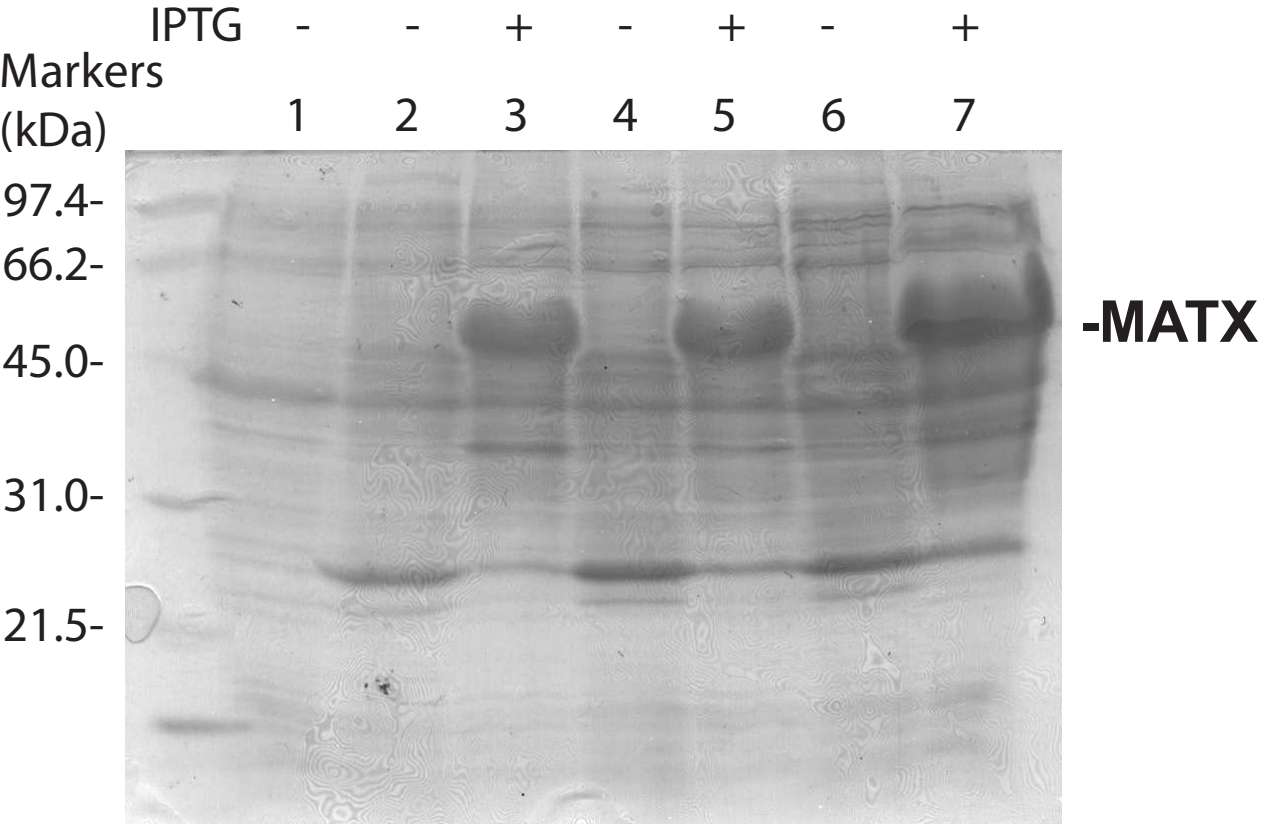
IPTG - - + - + - +
Markers
1 2 3 4 5 6 7
(kDa)
97.4-
66.2-
45.0-
31.0-
21.5-
-MATX

Figure 2

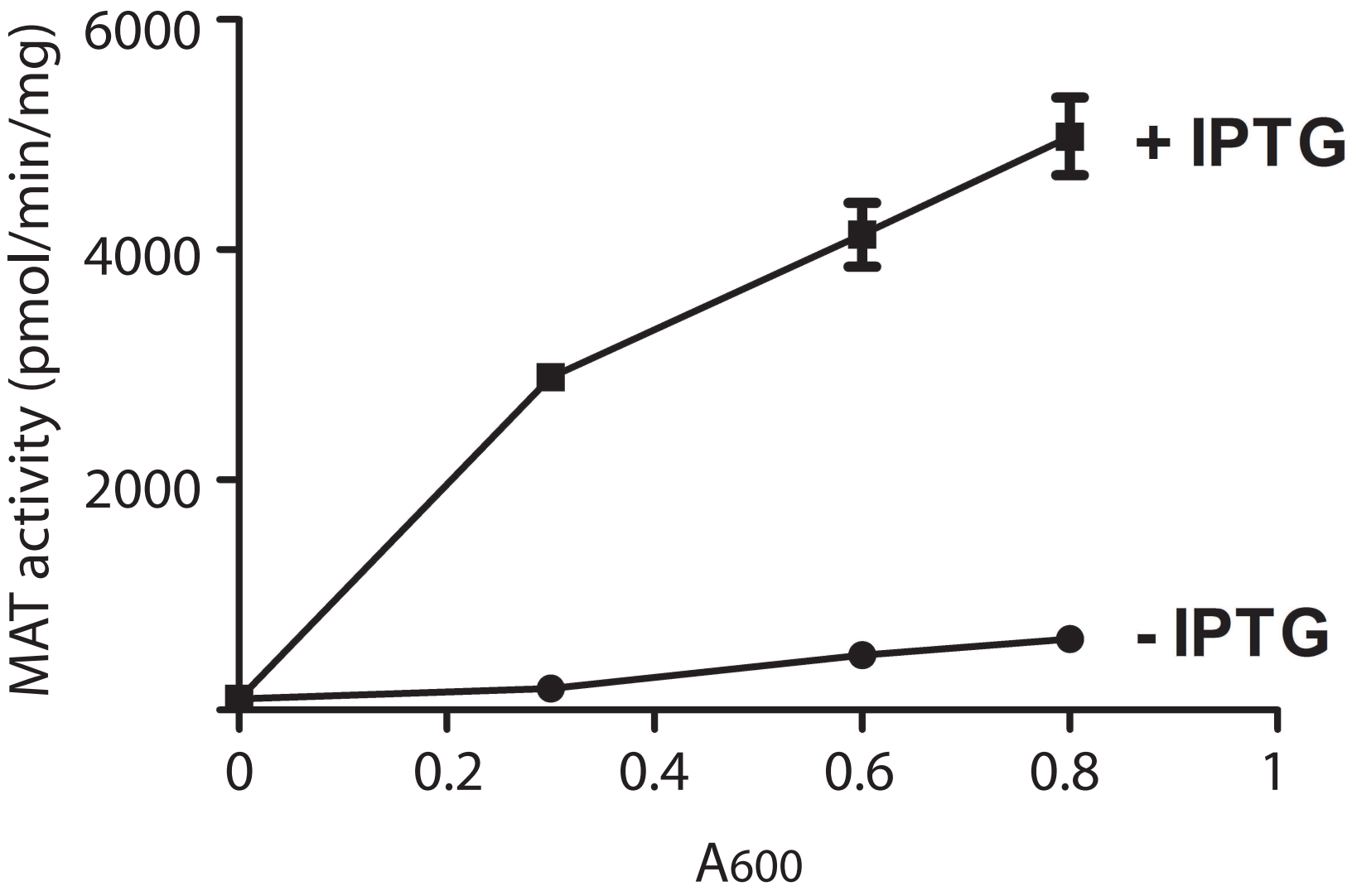
6000
4000
2000
MAT activity (pmol/min/mg)
+ IPTG
- IPTG
0
0.2
0.4
0.6
0.8
1
A600

Figure 3

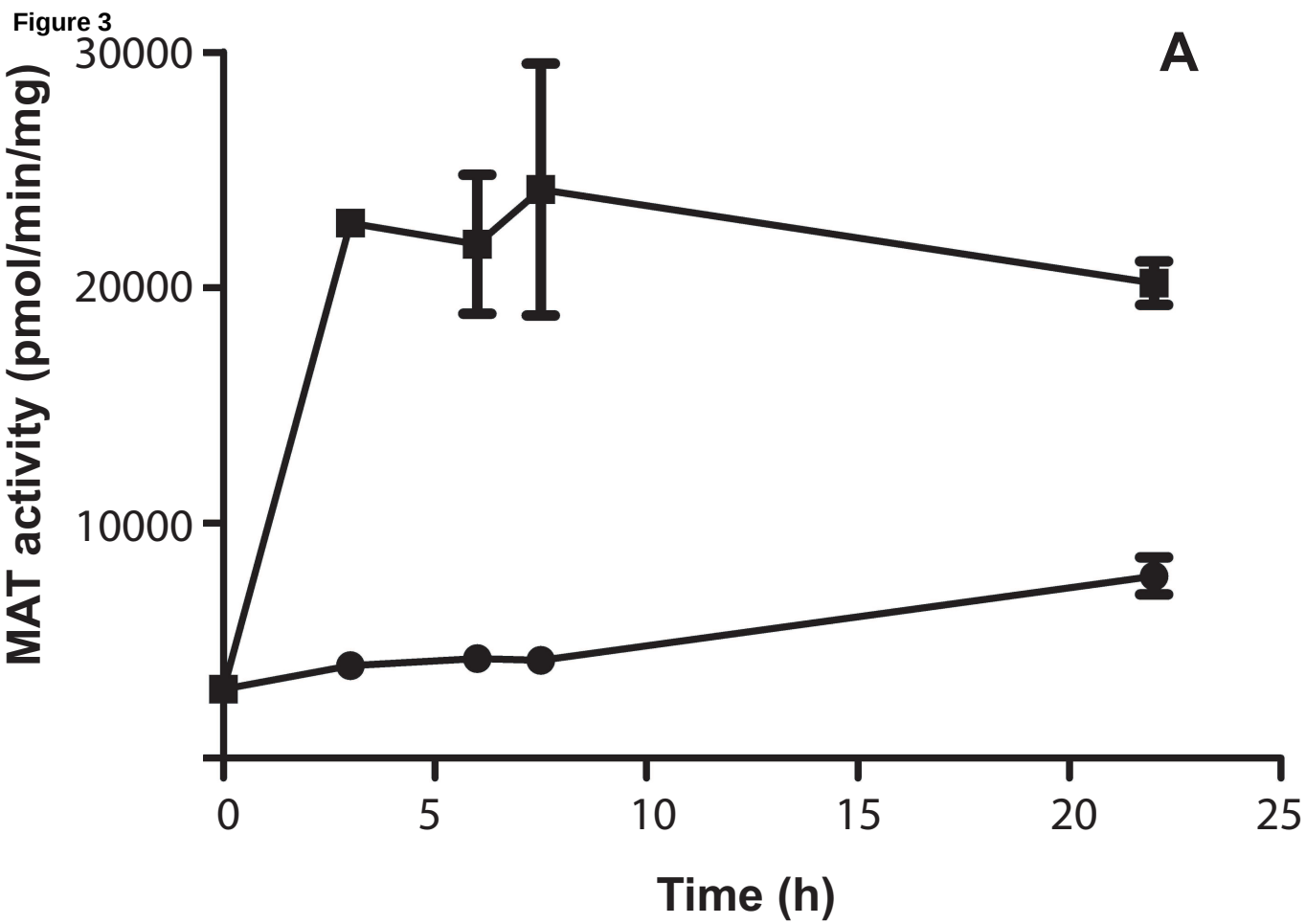
A
MAT activity (pmol/min/mg)
30000
20000
10000
0
5
10
15
20
25
Time (h)

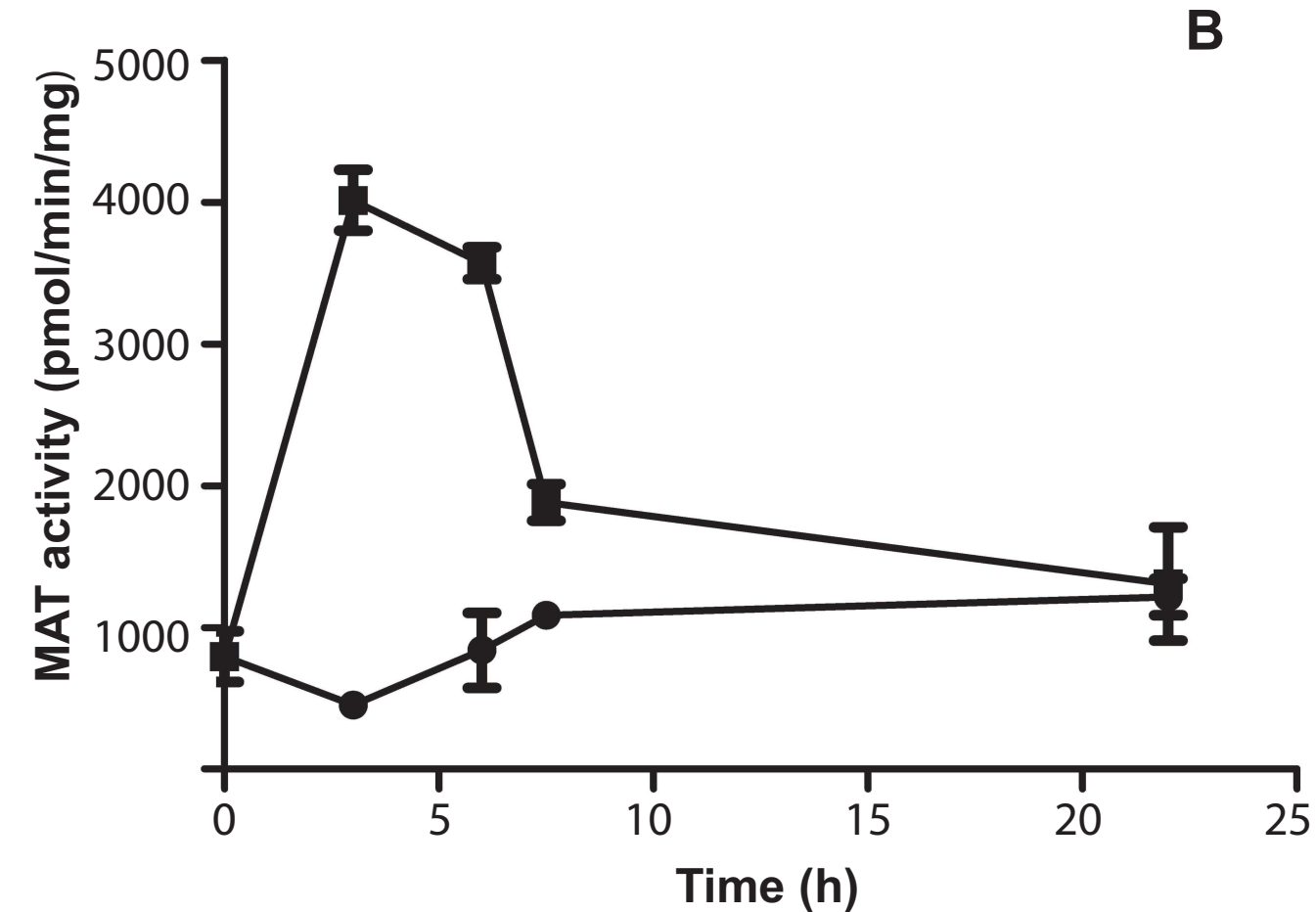
B
MAT activity (pmol/min/mg)
5000
4000
3000
2000
1000
0
5
10
15
20
25
Time (h)

Figure 4

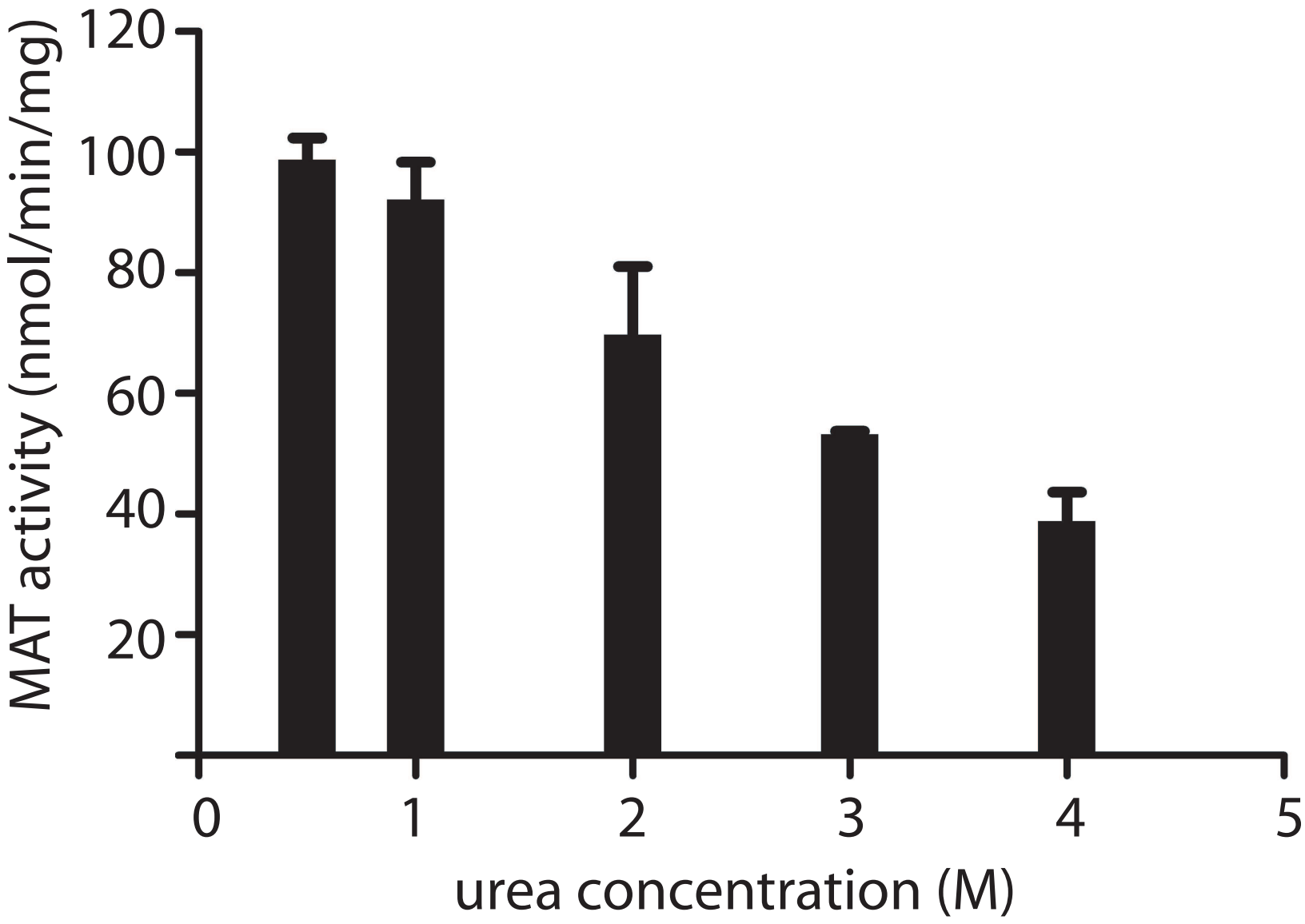
MAT activity (nmol/min/mg)
120
100
80
60
40
20
0
1
2
3
4
5
urea concentration (M)

Figure 5

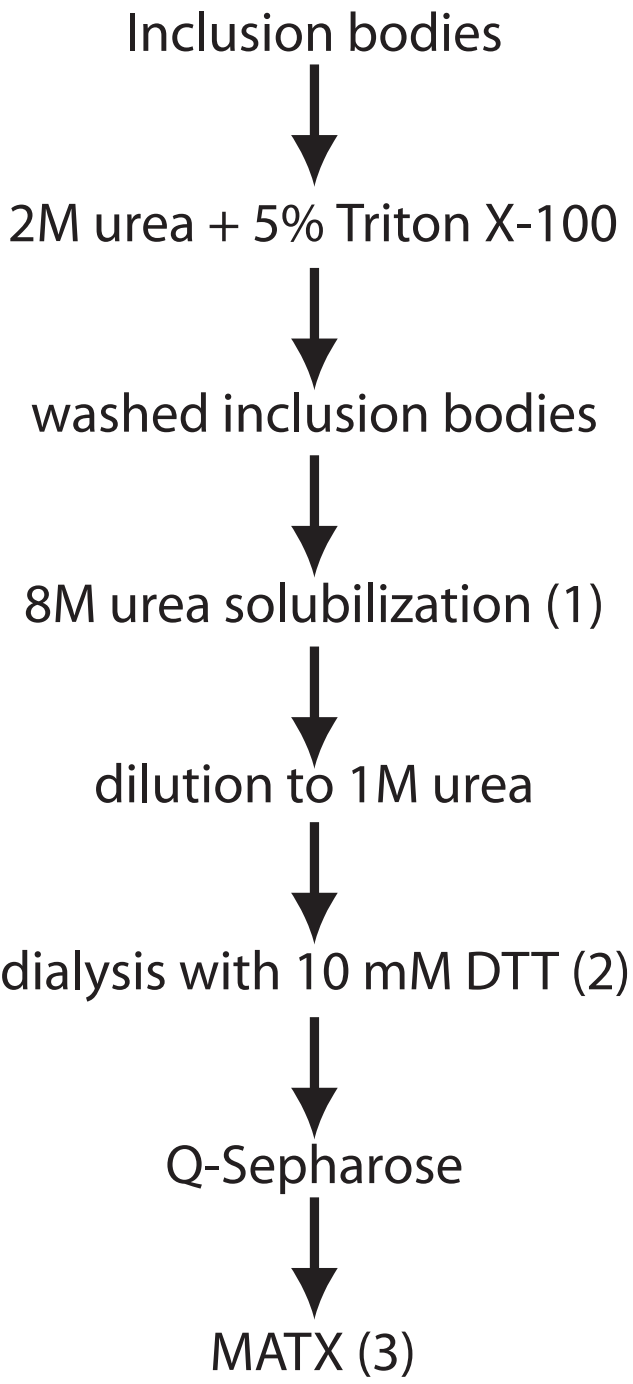
Inclusion bodies
2M urea + 5% Triton X-100
washed inclusion bodies
8M urea solubilization (1)
dilution to 1M urea
dialysis with 10 mM DTT (2)
Q-Sepharose
MATX (3)

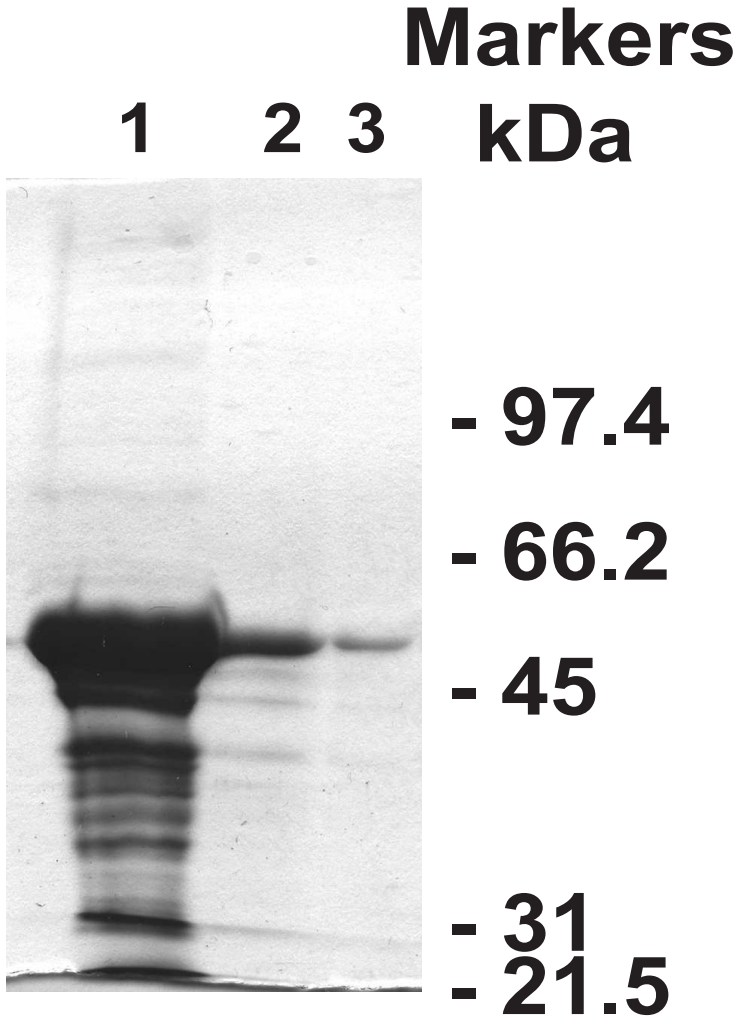
Markers
1
2
3
kDa
- 97.4
- 66.2
- 45
- 31
- 21.5

Figure 6

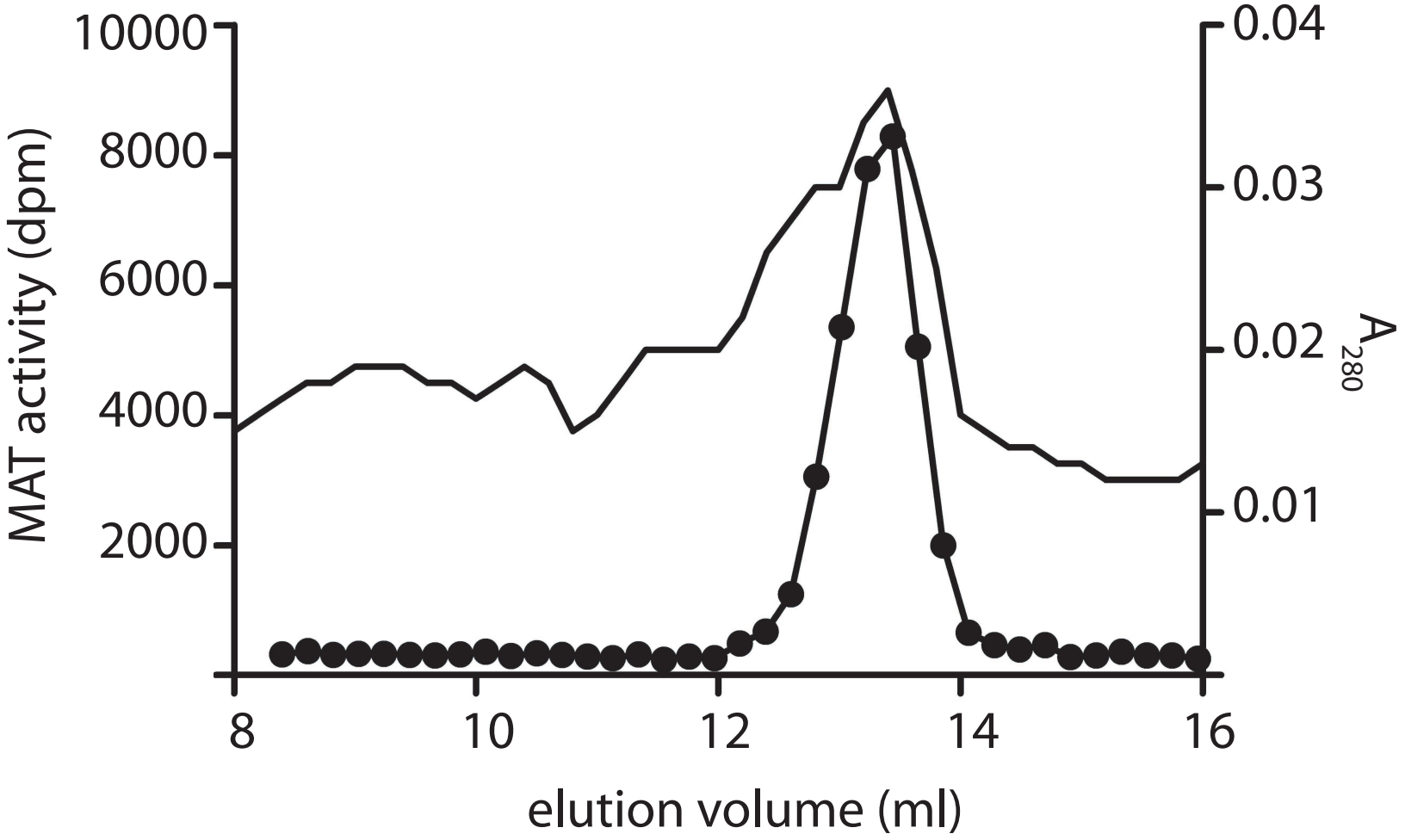
10000
8000
6000
4000
2000
MAT activity (dpm)
0.04
0.03
0.02
0.01
A280
8
10
12
14
16
elution volume (ml)

Figure 7

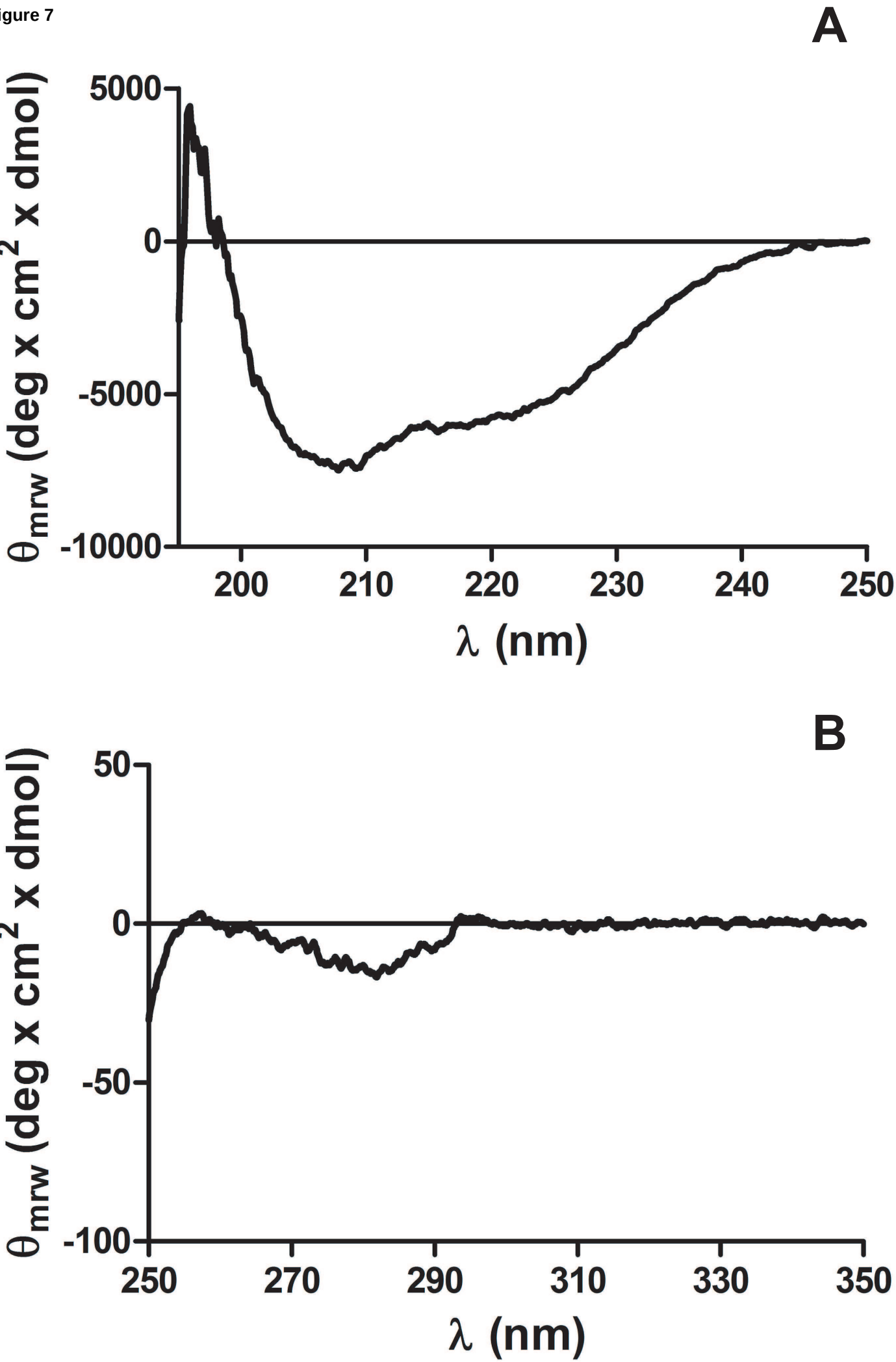
A
5000
0
-5000
-10000
θmrw (deg x cm2 x dmol)
200
210
220
230
240
250
λ (nm)
B
50
0
-50
-100
θmrw (deg x cm2 x dmol)
250
270
290
310
330
350
λ (nm)

Figure 8

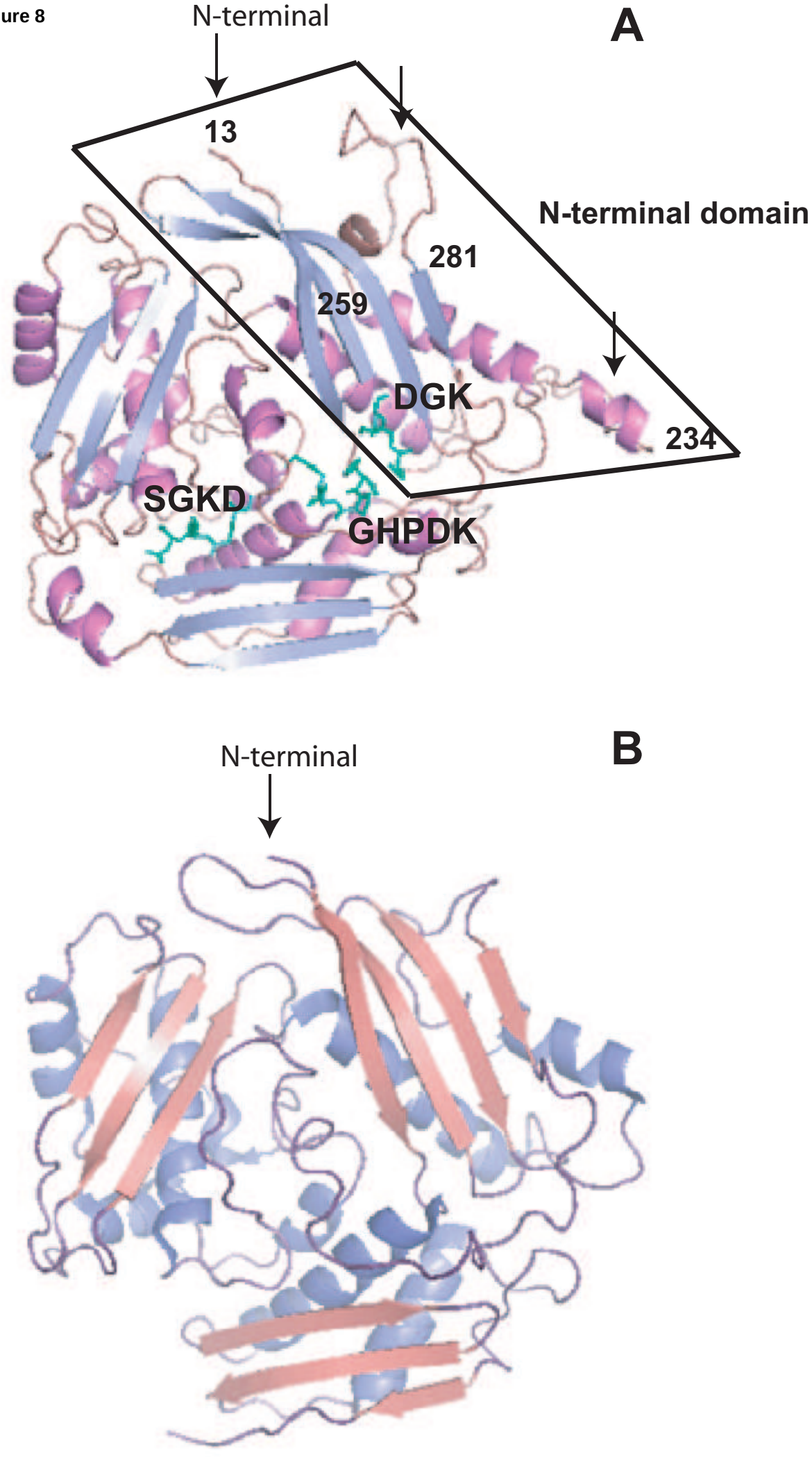
A
N-terminal
13
281
259
N-terminal domain
DGK
234
SGKD
GHPDK
B
N-terminal

Figure 8C

Click here to download high resolution image